Leakage and Resonance Characteristics of Radiating Cylindrical Dielectric Structure Suitable for Use as a Feeder for High-Efficient Omnidirectional/Sectorial Antenna

Songxin Qi and Ke Wu, *Senior Member, IEEE*

***Abstract*—A class of new radiating cylindrical dielectric structures are proposed for use as a feeder for high-efficient omnidirectional/sectorial slotted arrays that are suitable for high-frequency wireless systems. A simple and efficient model on a scheme of the method of lines is developed and used for analysis of these composite cylindrical dielectric elements that have various rectangular and trapezoidal cross sections. Good agreement between calculated and measured results is observed, which validates the proposed modeling technique. Leakage and resonance characteristics are presented, and they reveal some interesting features for design of new beamforming networks or circuits using the new structure. Results and discussion are focused on the properties of low-order leaky resonant modes. Influences of various parameters of the structure on leakage loss and resonant frequency are shown in detail for design purposes.**

***Index Terms*—Antenna feeder, dielectric resonator, leaky wave, numerical modeling.**

I. Introduction

THE ever-increasing demand for high-efficient, high-gain, low-profile, and low-cost antennas required by high-speed wireless systems has stimulated a great deal of interests searching for various feeder structures. These systems may operate at millimeter-wave frequencies, e.g., customer promises equipment (CPE) for local multipoint distribution service/local multipoint communication service (LMDS/LMCS), short-haul personal communication systems/local area networks (PCS's/LAN's), and collision-avoidance sensor. Although planar techniques present a number of advantages, namely, low-profile, lightweight, and conformable geometry, they suffer from inherently significant ohmic loss at millimeter-wave frequencies, especially in connection with a high-gain requirement. This deficiency greatly reduces the radiation efficiency, and also degrades the noise performance of a receiver system [1], [2]. In parallel, a leaky-wave structure derived from the nonradiative dielectric waveguide (NRD-guide) [3] has been shown to offer a number of unmatched advantageous features in the design of an antenna feeder for use at higher frequencies due to its low loss, very flexible radiation characteristics, and mechanical simplicity [4], [5].

Over the past years, various leaky-wave NRD structures or similar radiating elements have been proposed, such as routing the dielectric strip close to the open-end of a metallic plate in [6], using a trapezoidal strip to cause a radiating mode in [7], adopting a periodic array of grooves on the upper surface of dielectric strip in [8], modifying a dielectric-inset structure with a double-strip grating in [9], and relocating an NRD resonator in the proximity of the open aperture (unidirectional dielectric radiator) [4], [10]. All these measures are actually stemmed from an appropriate geometrical modification of the uniform NRD-guide or resonator. In this paper, a new class of leaky-wave-related cylindrical dielectric resonant structures are proposed for use in the design of feeder for cylindrical slotted-array antennas operating at millimeter-wave frequencies. Theoretical analysis and experimental verification are presented for showing technical features of the new structures. In particular, complex resonant frequency and its parametric effects are obtained for a number of the radiating elements shaped for various design purposes.

II. Modeling of New Radiating Structures

A. Description of the Proposed Radiating Structure

As shown in Fig. 1, cylindrical dielectric structures with various rectangular or trapezoidal cross sections are sandwiched between two parallel conducting plates, as in the case of an NRD-guide. This cylindrical geometry may be in the form of a multilayered composite ring. In such an arrangement, the structure has two possible states, namely, trapped and leaky states, depending on the operating modes and geometrical design. In a leaky state, a certain portion of electromagnetic energy leaks continuously away from the resonator along the radial direction. In other words, the radiation takes place omnidirectionally over the cross section. Fig. 1(a) and (b) shows two potential geometrical arrangements for designing a multistacked leaky-wave feeder for microwave and millimeter-

Manuscript received December 15, 1997; revised June 2, 1998. This work was supported by the Natural Sciences and Engineering Research Council (NSERC) of Canada.

S. Qi was with Polygrames Research Center, Department of Electrical and Computer Engineering, Ecole Polytechnique, Montréal, P.Q., Canada H3C 3A7. He is now with the Broadband Wireless Networks Division, Northern Telecom (Nortel) Corporation, Winnipeg, Man., Canada R3H 0H9

K. Wu is with Polygrames Research Center, Department of Electrical and Computer Engineering, Ecole Polytechnique, Montréal, P.Q., Canada H3C 3A7.

Publisher Item Identifier S 0018-9480(98)08007-7.

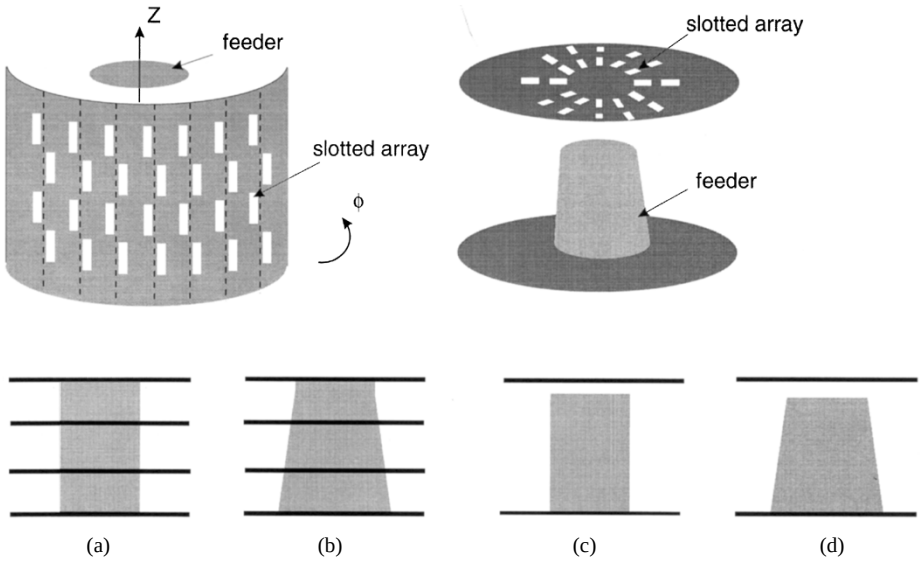

Fig. 1. Cross-sectional view of a class of potentially radiating cylindrical composite dielectric-resonator structures for use as a feeder for cylindrically slotted-array antennas. The proposed resonators may consist of rod and ring topologies. (a) Multistacked regular shaped resonator. (b) Multistacked trapezoidal resonator. (c) Regular resonator with air gap. (d) Trapezoidal resonator with air gap.

wave antennas. In Fig. 1(c) and (d), an air gap is intentionally designed between the dielectric resonator and one of the metallic plates, which is in direct connection with the degree of such a leakage as well as resonant modes [11]. In this way, all the trapped modes can be converted gradually into the leaky states, which is very important to design the signal-feeding architecture for the antenna array to yield and expect beamforming performance.

Such leakage characteristics may allow one to design a feeder of cylindrically conformable slotted-array antennas for millimeter-wave applications if the leaky-mode resonator is placed at the center of such a cylindrical disk. As shown schematically in Fig. 1, the slotted-array antennas consist of one of the cylindrical conducting plate etched with a (large) number of slots spread over the complete cylindrical plane, which are fed progressively along the radial direction by the leakage source generated by the resonator. Clearly, the design of such an array antenna depends on the degree of the power leakage (leaky-wave factor), the profile of the slot arrays (dimension and geometry), as well as resonance characteristics of the dielectric resonator. Therefore, a good understanding of the leakage and resonance characteristics featuring various parametric effects and geometrical shapes are mandatory for effective performance analysis and successful design of an application-specific array antenna such as a high-gain requirement.

As opposed to the conventional NRD leaky-wave guide, the new structure offers some complementary advantages. The leaky resonant mode desired with an excellent omnidirectional radiation pattern can be easily induced, and its operating frequency and radiation impedance may be controlled by adjusting the spacing between the two conducting plates. The latter aspect is of great importance for a practical design. Naturally, the cross-sectional shape and other parameters of structure should also be considered as very important design aspects.

In the cylindrical coordinate system, as indicated in Fig. 1, any possible resonance may take place with three possible kinds of modes with reference to the z-direction: TE, TM, and hybrid modes. In this paper, only the low-order resonant modes will be studied and discussed. Under a leaky state, the free-running oscillating phenomena can be simply described by a complex resonant frequency. Electromagnetic fields have a time dependence $\exp(j\omega t)$ in which the angular resonant frequency $\omega = \omega_r + j\omega_i$. In this complex frequency term, $\omega_r > 0$ is the oscillating frequency (operating frequency), while $\omega_i > 0$ stands for the decay factor (or energy leakage rate). This is rather different from the guided-wave leakage, as in the case of a leaky-wave NRD-guide for which the leaky-wave factor is defined by the attenuation factor (loss) of the propagation constant. In our case, the leaky-wave factor is represented by $\omega_i = 2\pi f_i$ (or f_i). Under certain circumstances, the leakage factor may also be judged from the resonance factor that is usually calculated from $\omega_r/(2\omega_i)$. In the following analysis and discussion, only $f = f_r + jf_i$ will be used for simplicity.

B. Leakage and Resonance Modeling of the Proposed Structure

Although some numerical techniques can be applied to leakage and resonance modeling of the proposed structure with arbitrary cross-sectional shape [12], [13], a simple and efficient algorithm is developed in this paper with the semianalytical scheme of the method of lines formulated in the cylindrical coordinate. This technique is well known for its efficiency and effectiveness compared to its counterparts for this kind of structures.

As indicated in Fig. 1, the proposed cylindrical leaky resonant structures may have inhomogeneous layers featuring a space variable dependence of permittivity $\varepsilon_r(z)$. The modal electromagnetic fields can be described by two z-oriented potential functions ψ^e and ψ^h, which should satisfy both

Helmholtz and Sturm–Liousville differential equations, respectively, such that

$$\frac{1}{\rho}\frac{\partial}{\partial\rho}\left(\rho\frac{\partial\psi^e}{\partial\rho}\right)+\frac{1}{\rho^2}\frac{\partial^2\psi^e}{\partial\varphi^2}+\varepsilon_r(z)\frac{\partial}{\partial z}\left(\varepsilon_r^{-1}(z)\frac{\partial\psi^e}{\partial z}\right)+\varepsilon_r(z)k_0^2\psi^e=0$$
$$\frac{1}{\rho}\frac{\partial}{\partial\rho}\left(\rho\frac{\partial\psi^h}{\partial\rho}\right)+\frac{1}{\rho^2}\frac{\partial^2\psi^h}{\partial\varphi^2}+\frac{\partial^2\psi^h}{\partial z^2}+\varepsilon_r k_0^2\psi^h=0. \quad (1)$$

The electric- and magnetic-field components in cylindrical coordinate are derived from

$$\vec{E}=\nabla\times\nabla\times(\psi^e\vec{u}_z)/j\omega\varepsilon-\nabla\times(\psi^h\vec{u}_z)$$
$$\vec{H}=\nabla\times(\psi^e\vec{u}_z)+\nabla\times\nabla\times(\psi^h\vec{u}_z)/j\omega\mu_0 \quad (2)$$

and, e.g.,

$$E_z=\frac{1}{j\omega\varepsilon_r(z)}\left[\varepsilon_r(z)k_0^2\psi^e+\varepsilon_r(z)\frac{\partial}{\partial z}\left(\varepsilon_r^{-1}(z)\frac{\partial\psi^e}{\partial z}\right)\right]. \quad (3)$$

A nonequidistant discretization scheme along the z-direction is applied to the above differential equations considering the boundary conditions related to the two metal plates and the homogeneity in the azimuthal direction (φ) with

$$\frac{\partial^2\psi^{e,h}}{\partial\varphi^2}=-n^2\psi^{e,h} \quad (4)$$

where n denotes the modal order in the φ rotated orientation. As usual, two sets of a discrete line system in relation to ψ^e and ψ^h can be arranged as shown in Fig. 2, interlaced with each other, where the magnetic lines should coincide with different dielectric interfaces. The effect of the inhomogeneity can be effectively accounted for by setting up diagonal matrices $\bar{\varepsilon}_r^{e,h}$ in the discrete domain. The discretization scheme of ε_r^h at an interface (see Fig. 2) where there is a dielectric discontinuity is defined by

$$\varepsilon_G=\varepsilon_r^h\big|_{\text{interface}}=\frac{\varepsilon_{r1}h_1+\varepsilon_{r2}h_2}{h_1+h_2}. \quad (5)$$

Therefore, the second-order derivatives of ψ^e across the interface can be written as (6), shown at the bottom of this page. As detailed in [14] and [15], two orthogonal matrix transformations are applied to the discrete (vector or matrix) form of (1) with $\bar{\psi}^{e,h}=T^{e,h}\tilde{\psi}^{e,h}$. Both Helmholtz and Sturm–Liouville equations are now cast into the following uncoupled ordinary differential matrix equation in the transform domain:

$$\rho\frac{\partial}{\partial\rho}\left(\rho\frac{\partial\tilde{\psi}^{e,h}}{\partial\rho}\right)+\left[\left(\bar{k}_\rho^{e,h}\rho\right)^2-n^2I^{e,h}\right]=0 \quad (7)$$

with

$$\left(\bar{k}_\rho^{e,h}\right)^2=(T^{e,h})^{-1}\big(\underbrace{k_0^2\bar{\varepsilon}_r^{e,h}-P^{e,h}}_{Q^{e,h}}\big)T^{e,h}$$

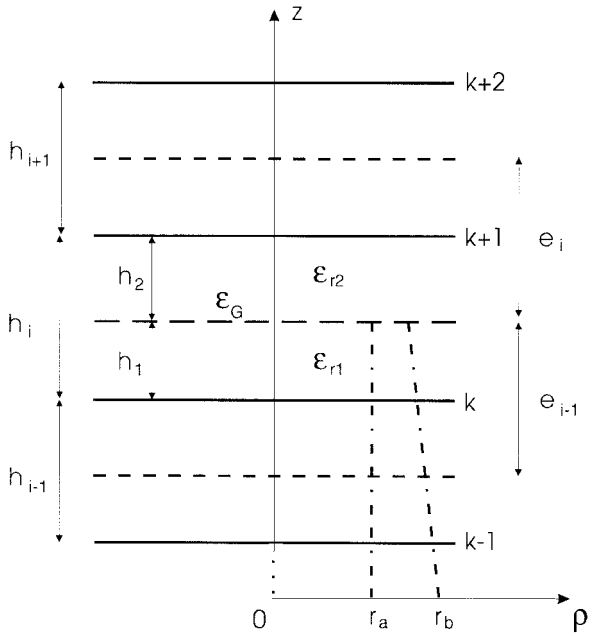

Fig. 2. Discretization scheme and abrupt transition of ψ^e from ε_{r1} to ε_{r2} handled in the cylindrical-coordinate method of lines.

where k_0 is the free-space propagation, $I^{e,h}$ is the unit matrix, $P^{e,h}$ is the difference operators for the second-order derivatives [14], which implicitly involve the difference operator $D^{e,h}$ for the first-order derivatives. The resulting matrices $\bar{k}_\rho^{e,h}$ are diagonal and contain the propagation constant in the radial direction.

Considering an arbitrary cylindrical dielectric layer with a thickness $d^{e,h}=r_b^{e,h}-r_a^{e,h}$, as shown in Fig. 2, the above equations have the following well-known solution:

$$\rho\frac{\partial}{\partial\rho}\begin{bmatrix}\tilde{\psi}^{e,h}\big|_{r_a^{e,h}}\\ \tilde{\psi}^{e,h}\big|_{r_b^{e,h}}\end{bmatrix}=\Omega_n^{e,h}\cdot\begin{bmatrix}\chi_n^{e,h} & -\frac{2j}{\pi}I^{e,h}\\ \frac{2j}{\pi}I^{e,h} & s_n^{e,h}\end{bmatrix}\cdot\begin{bmatrix}\tilde{\psi}^{e,h}\big|_{r_a^{e,h}}\\ \tilde{\psi}^{e,h}\big|_{r_b^{e,h}}\end{bmatrix} \quad (8)$$

with

$$\Omega_n^{e,h}=\left[J_n\left(\bar{k}_\rho^{e,h}r_a^{e,h}\right)\cdot H_n^{(2)}\left(\bar{k}_\rho^{e,h}r_b^{e,h}\right)-J_n\left(\bar{k}_\rho^{e,h}r_b^{e,h}\right)\cdot H_n^{(2)}\left(\bar{k}_\rho^{e,h}r_a^{e,h}\right)\right]^{-1}_{\text{diag}}$$
$$\chi_n^{e,h}=\bar{k}_\rho^{e,h}r_a^{e,h}\cdot\left[J_n'\left(\bar{k}_\rho^{e,h}r_a^{e,h}\right)\cdot H_n^{(2)}\left(\bar{k}_\rho^{e,h}r_b^{e,h}\right)-J_n\left(\bar{k}_\rho^{e,h}r_b^{e,h}\right)\cdot H_n'^{(2)}\left(\bar{k}_\rho^{e,h}r_a^{e,h}\right)\right]_{\text{diag}}$$
$$s_n^{e,h}=\bar{k}_\rho^{e,h}r_b^{e,h}\cdot\left[J_n\left(\bar{k}_\rho^{e,h}r_a^{e,h}\right)\cdot H_n'^{(2)}\left(\bar{k}_\rho^{e,h}r_b^{e,h}\right)-J_n'\left(\bar{k}_\rho^{e,h}r_b^{e,h}\right)\cdot H_n^{(2)}\left(\bar{k}_\rho^{e,h}r_a^{e,h}\right)\right]_{\text{diag}}$$

in which $J_n(\bar{k}_\rho^{e,h}\rho^{e,h})$ and $H_n^{(2)}(\bar{k}_\rho^{e,h}\rho^{e,h})$ are a Bessel function of the first kind and Hankel function of the second kind, respectively.

$$\left.\frac{d}{dz}\left(\frac{1}{\varepsilon_{r1}}\frac{d\psi^e}{dz}\right)\right|_k=\frac{1}{e_{i-1}}\left[\frac{1}{\varepsilon_{r1}h_{i-1}}\psi_{k-1}^e-\left(\frac{1}{\varepsilon_{r1}h_{i-1}}+\frac{1}{\varepsilon_G h_i}\right)\psi_k^e+\frac{1}{\varepsilon_G h_i}\psi_{k+1}^e\right]$$
$$\left.\frac{d}{dz}\left(\frac{1}{\varepsilon_{r2}}\frac{d\psi^e}{dz}\right)\right|_{k+1}=\frac{1}{e_i}\left[\frac{1}{\varepsilon_G h_i}\psi_k^e-\left(\frac{1}{\varepsilon_{r2}h_{i+1}}+\frac{1}{\varepsilon_G h_i}\right)\psi_{k+1}^e+\frac{1}{\varepsilon_{r2}h_{i+1}}\psi_{k+2}^e\right] \quad (6)$$

A simple matrix relationship of the tangential-field components E_z, E_φ, H_z, and H_φ between two different locations in the same dielectric layer in the radial direction can be obtained as follows:

$$\begin{pmatrix} H_a \\ H_b \end{pmatrix} = \begin{bmatrix} Y_a & Y_t \\ Y_t & Y_b \end{bmatrix} \cdot \begin{pmatrix} E_a \\ E_b \end{pmatrix} \tag{9}$$

with the following abbreviations:

$$H_{a,b} = j\eta_0 \begin{bmatrix} H_z|_{r_{a,b}} \\ r_{a,b}H_\varphi|_{r_{a,b}} \end{bmatrix} \quad E_{a,b} = \begin{bmatrix} r_{a,b}E_\varphi|_{r_{a,b}} \\ E_z|_{r_{a,b}} \end{bmatrix}. \tag{10}$$

Equation (9) consists of submatrices Y_a, Y_b, and Y_t, which are given in the Appendix.

In order to formulate an indirect eigenvalue problem, we impose the above-described continuity condition at each dielectric interface and then successively manipulate a set of matrix equations starting from the inner region. With (9), the following typical equation can be derived for the interface at r_b, e.g.,

$$H_b^{(l)} = Y^{(l)} \cdot E_b^{(l)} \tag{11}$$

with $Y^{(l)}$ defined recursively as

$$Y^{(l)} = Y_t^{(l)}\left(Y_a^{(l)} - Y^{(l-1)}\right)^{-1} Y_t^{(l)} - Y_b^{(l)}. \tag{12}$$

Invoking the remaining continuity condition, a trivial-field coefficient characteristic matrix is obtained, and the complex resonant frequency can be easily solved by

$$\det[G(f)] = 0. \tag{13}$$

In this way, the leakage and resonance characteristics can be derived with a series of calculations. In addition, the field profiles can also be calculated by a technique of singular-value decomposition (SVD) if necessary.

III. Results and Discussion

Based on the above-described technique, an algorithm for calculating the complex resonant frequency is developed and the proposed leaky-wave cylindrical dielectric resonant structures with various cross sections are studied as follows. To verify our modeling technique, an X-band resonator discussed in [13] is calculated and its results are presented in Table I, showing a special case of our proposed geometries. A good agreement is observed between our results and those presented in [13]. In addition, a measurement for the low-order modes is also made in this paper and experimental results further confirm the validity and accuracy of our model.

An appropriate classification of modes in the proposed cylindrical structures is usually difficult, considering different possible cross sections and the existence of an air gap. In the following analysis, the modes of interest are designated as $\mathrm{TE}_{0m\delta}$, $\mathrm{TM}_{0m\delta}$, and $\mathrm{HEM}_{nm\delta}$ for the three sets of z-oriented TE, TM, and hybrid modes in the coordinate (ρ, φ, z). The first subscript n herewith features the variation of modal fields in the φ direction while the second presents the order of resonant frequency, and the third special index refers to a fraction of half-period field variation along the z-axis (this is usually the case for an asymmetric structure in the z-direction).

TABLE I
General Comparison Among the Calculated Resonant Frequency Compared with Our Measurements and Results Obtained by Using a Boundary-Element Method for the Low-Order Modes of an NRD Resonator Having a Circular Section (Rod Resonator Structure) of Radius $R = 11$ mm and a Fixed Height $H = 12.3$ mm with a Relative Dielectric Permittivity $\varepsilon_r = 2.53$. (Note That All the Calculations Are Carried Out by Setting a Relative Numerical Accuracy of 10^{-18} for Bessel and Henkel Functions and 10^{-8} for (13), and Discretization of 15 e-Lines Along the z-Direction)

Modes	This approach (GHz)	BEM [13] (GHz)	Measured (GHz)	Error (%)
$HEM_{11\delta}$	9.223	9.226	9.24	-0.18
$TE_{01\delta}$	10.098	10.098	10.11	-0.12
$TM_{01\delta}$	11.134	11.137	11.13	0.03
$HEM_{21\delta}$	11.334	11.335	11.37	-0.32

To simplify the following discussion, two dielectric materials (Polystyrene $\varepsilon_r = 2.53$ and Rogers' $\mathrm{TMM3}^{\mathrm{TM}} \varepsilon_r = 3.27$) are considered in this paper and calculations are presented for basic resonant structures operating at X- and Ku-bands. With such a consideration, the spacing of the two metal plates is selected according to the basic requirement of the NRD-guide, which guarantees a nonradiative condition if the structure is symmetric with reference to the z-axis. Fig. 3(a) and (b) plots low-order-mode charts for different trapezoidal dielectric structures as a function of the trapezoidal angle θ. Naturally, the low permittivity dielectric resonance occurs at higher frequency than its high permittivity counterpart, as shown in Fig. 3. It is observed that the resonant frequency of $\mathrm{TE}_{01\delta}$, $\mathrm{TM}_{01\delta}$, $\mathrm{HEM}_{11\delta}$, and $\mathrm{HEM}_{21\delta}$ shows a slight increase with θ in the trapped state while the resonance of $\mathrm{HEM}_{31\delta}$ in the leaky state is much more pronounced. Its leakage characteristics are depicted in Fig. 4 through the imaginary part of the complex resonant frequency, indicating that the leakage factor is significantly affected by θ. This implies that the quality factor decreases and the structure becomes more radiative if $\mathrm{HEM}_{31\delta}$ is selected as the operating mode. This mode is radiative even for the symmetric topology $(\theta = 0)$. This feature is interesting for antenna feeder design, which usually requires the leakage level for an appropriate power delivery between the two metal plates along the radial direction. Usually, the feature (modal profile) of a free-running resonance in a trapped state remains relatively stationary with θ. This suggests that an appropriate leaky resonant mode can be obtained by choosing a specific structure with a correct excitation. It is very important to point out that a useful leakage between the two plates is usually expected to be in the form of a TEM-mode propagation, as in the case of a leaky-wave NRD-guide. Nevertheless, any leakage other than TEM-mode propagation generated by a structure may also be useful for the design of a feeder as long as the signal-feeding architecture yields an expected beamforming performance for the designated antenna array.

As for cylindrical dielectric structures with an air gap between the dielectric and one of the conducting plates, as shown in Figs. 1(c) and (d), a trapped state can be effectively

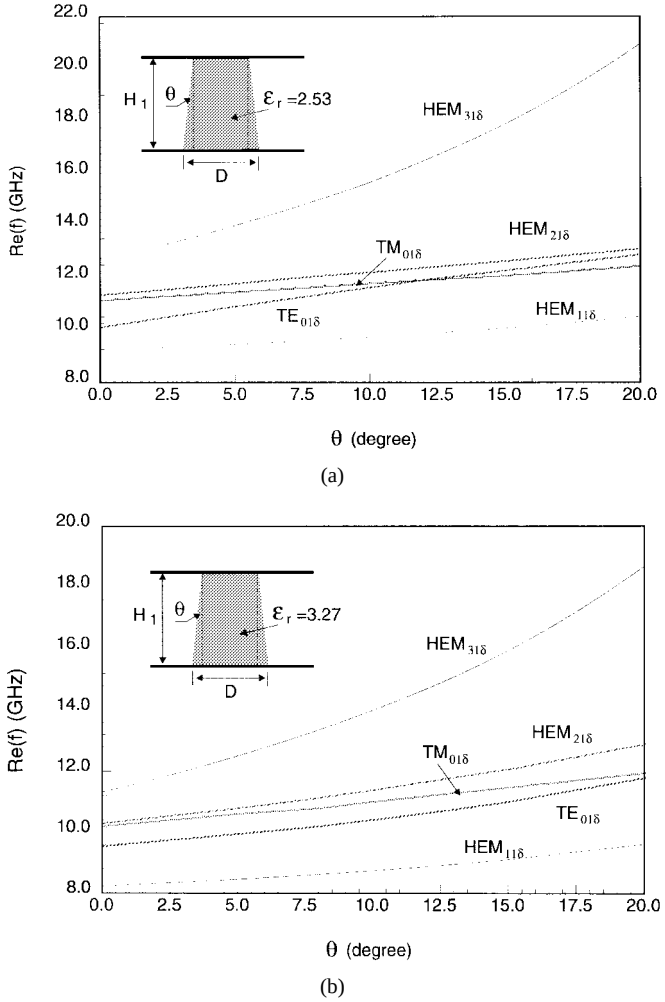

Fig. 3. Resonant frequency (trapped state) of low-order modes versus the trapezoidal angle of dielectric resonators with $D = 22$ mm, $H_1 = 12.3$ mm. (a) In the case of Polystyrene material, $\varepsilon_r = 2.53$. (b) In the case of Rogers TMM-3 material, $\varepsilon_r = 3.27$.

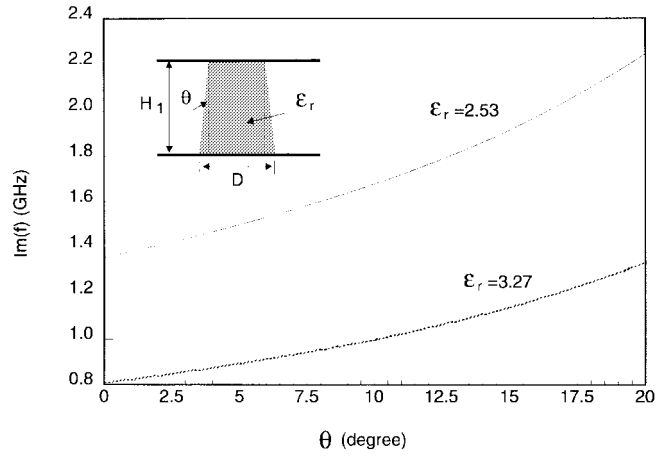

Fig. 4. Leakage characteristics of $\mathrm{HEM}_{31\delta}$ mode versus the trapezoidal angle of dielectric resonators with the two different permittivities.

converted into a leaky state. Fig. 5 shows the influence of the air-gap height on the resonant frequency and leakage characteristics of $\mathrm{HEM}_{11\delta}$ mode (converted to the trapped state) for both dielectric rod ($R = 0$ mm) and ring ($R =$

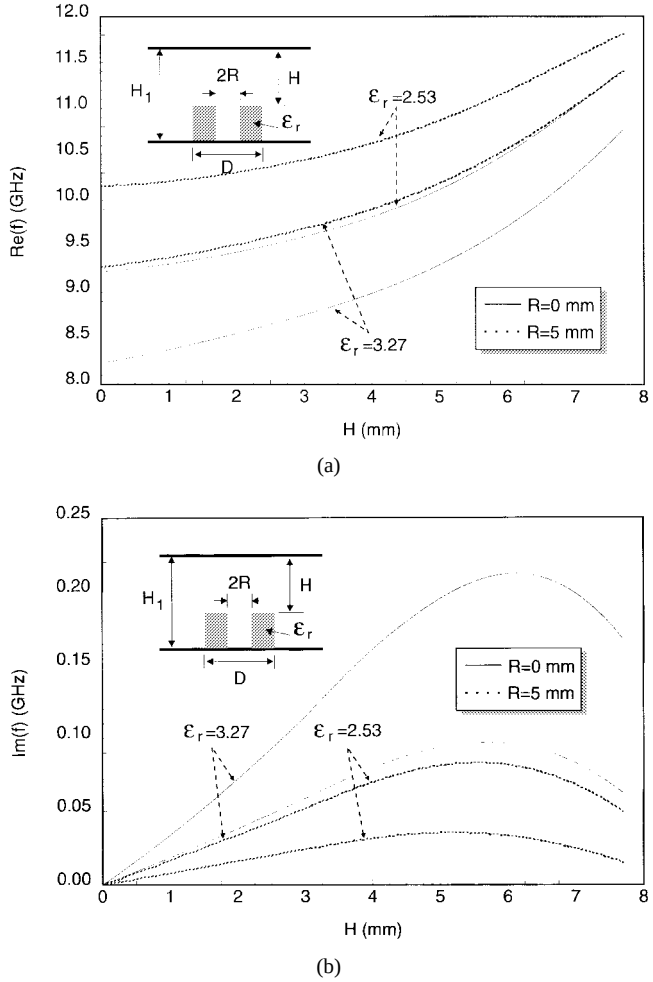

Fig. 5. Effects of the air-gap size on (a) resonant frequency and (b) leaky factor of $\mathrm{HEM}_{11\delta}$ for dielectric rod ($R = 0.0$ mm) and ring ($R = 5.0$ mm) with the two different permittivities ($D = 22$ mm, $H_1 = 12.3$ mm).

5 mm) resonators while the space between the plates is fixed ($H_1 = 12.3$ mm). Note that the ring structure may provide an alternative for potential feeder design. An interesting feature is observed in Fig. 5(b) in that the leakage reaches its maximum value around $H = 6.0$ mm for this specific geometry, meaning a strong radiation. It is also found that the maximum values for the two dielectric materials are offset slightly from each other. In our case study, a higher dielectric permittivity provides a higher radiation and the rod resonator is a radiator better than its ring counterpart. On the other hand, the leaky resonance, as indicated in Fig. 5(a), shows that a structure with lower dielectric permittivity provides a higher frequency resonance as opposed to its leakage characteristics. The ring resonator also has a higher frequency resonance. In any case, it is not surprising to find out that the resonant frequency of a leaky resonance always shows a monotone increase with the air gap, and such an increase seems to be accelerated once the dimension of H goes beyond 6.0 mm (the value related to the maximum leakage).

To visualize the effect of dielectric-resonator size on the complex resonant frequency, Fig. 6 gives a series of curves for the resonant frequency and leakage factor of rod structure versus the radius R in the case of a fixed air gap. Generally

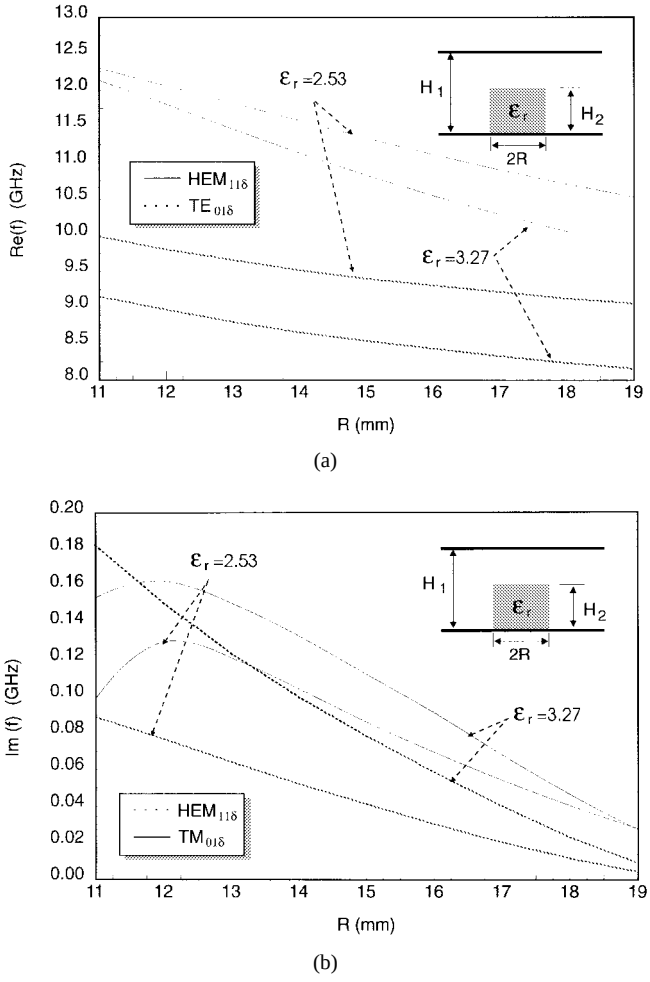

Fig. 6. Influence of the radius of (a) cylindrical dielectric rod resonators on resonant frequency and (b) leaky factor for $\mathrm{HEM}_{11\delta}$ and $\mathrm{TM}_{01\delta}$ with a fixed air-gap size such that $H_2 = 7.69$ mm ($D = 22$ mm, $H_1 = 12.3$ mm) in the case of considering the two different dielectric materials.

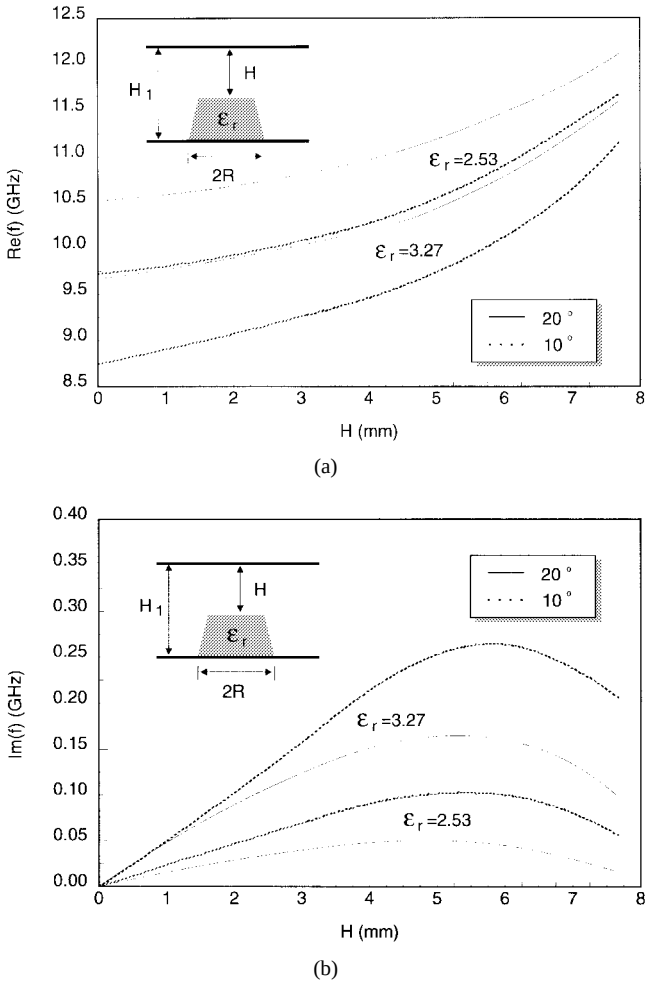

Fig. 7. $\mathrm{HEM}_{11\delta}$ related resonance and leakage characteristics of a trapezoidal rod in the presence of a variable air gap versus the two different angles for the two dielectric materials ($D = 22$ mm, $H_1 = 12.3$ mm). (a) Resonant frequency. (b) Leaky factor.

speaking, the resonant frequency and leakage factor tend to decrease with an increasing R for the two modes of interest $\mathrm{TM}_{01\delta}$ and $\mathrm{HEM}_{11\delta}$ even though an optimum leakage condition is found as $R = 12$ mm for the mode $\mathrm{TM}_{01\delta}$. This may indicate that an appropriate leaky mode can be generated by a carefully selected geometry.

To determine the shape effect of the proposed resonators on resonance and leakage, two separate figures of Fig. 7 plot a number of curves for the mode $\mathrm{HEM}_{11\delta}$, showing two special cases in connection with the trapezoidal cross section ($\theta = 10°$, and $\theta = 20°$) for the two dielectric materials in the presence of an air gap. Although a similar behavior of the leaky resonance is found between Fig. 5 (the rectangular cross section) and this case study, the trapezoidal profile has a significant impact on the resonant frequency and leakage factor. They are higher than those of the rectangular counterpart. Also, the maximum value of leakage is obtained around $H = 6$ mm. Interestingly, this may point to the fact that a maximum leakage (radiation) may take place if the height of a dielectric resonator is roughly or closely one-half of the spacing between the two plates for a given shape. It is seen in this example that a larger angle does not necessarily yield a stronger leakage and also that the maximum point may be shifted toward a smaller air gap.

IV. Conclusion

This paper presents a first-band analysis of composite cylindrical dielectric resonators having various cross sections, which are proposed for use as feeders in the design of cylindrically conformal slotted arrays suitable for high-frequency and high-efficient omnidirectional/sectorial antennas. A modeling strategy is developed with a scheme of the method of lines in the cylindrical coordinate for calculating the complex resonant frequency of the proposed topologies. This method is validated by our experiments and by a comparison with the available results for a special case.

Interesting features related to trapped resonance and leakage property are presented and discussed in detail for low-order modes. It is found that the trapped and leaky states are interrelated, and the trapped state may be effectively converted into its leaky state for a class of structures including dielectric rod and ring resonators. In this paper, parametric effects of the trapezoidal profile and air gap are studied along with a number of examples, which show that an optimum strong

$$Y_a = \begin{bmatrix} Q^h T^h \left(\gamma_n^h\right)^{-1} s_n^h (T^h)^{-1} & Q^h T^h \left(\gamma_n^h\right)^{-1} s_n^h (T^h)^{-1} (\bar{Q}^e)^{-1} \\ -\frac{n}{k_0 h} D^h T^h \left(\gamma_n^h\right)^{-1} s_n^h (T^h)^{-1} & \tau_a \end{bmatrix}$$

$$Y_b = \begin{bmatrix} Q^h T^h \left(\chi_n^h\right)^{-1} (T^h)^{-1} & Q^h T^h \chi_n^h (\bar{Q}^e)^{-1} \\ -\frac{n}{k_0 h} T^h \left(\chi_n^h\right)^{-1} (T^h)^{-1} & \tau_b \end{bmatrix}$$

$$Y_t = \frac{2j}{\pi} \begin{bmatrix} -Q^h T^h \left(\gamma_n^h\right)^{-1} (T^h)^{-1} & -Q^h T^h \left(\gamma_n^h\right)^{-1} (T^h)^{-1} (\bar{Q}^e)^{-1} \\ \frac{n}{k_0 h} D^h T^h \left(\gamma_n^h\right)^{-1} (T^h)^{-1} & \tau_t \end{bmatrix}$$

leakage (radiation) may be obtained with certain geometry. It is shown that a potential maximum can be generated by an air gap of which the height is roughly or closely one-half of the spacing between the two metals. It is also highlighted that a larger angle of the trapezoidal cross section does not necessarily yield a stronger leakage. Our paper suggests that the leakage may be generated not necessarily in the form of a TEM-mode propagation between the two metal plates, as shown in the case of a leaky-wave NRD-guide. This points to potential applications of fundamental and higher order modes related leakage in cylindrical structures for the beamforming network.

APPENDIX

As defined in (9), submatrices Y_a, Y_b, and Y_t are shown at the top of this page, with

$$\begin{aligned}
(\bar{Q}^e)^{-1} &= \frac{n}{k_0 h} \left(\bar{\varepsilon}_r^h\right)^{-1} D^e (Q^e)^{-1} \bar{\varepsilon}_r^e \\
\gamma_n^{e,h} &= \bar{k}_\rho^{e,h} r_a^{e,h} \cdot \bar{k}_\rho^{e,h} r_b^{e,h} \\
&\quad \cdot \left[J_n'\left(\bar{k}_\rho^{e,h} r_a^{e,h}\right) \cdot H_n'^{(2)}\left(\bar{k}_\rho^{e,h} r_b^{e,h}\right) \right. \\
&\quad \left. - J_n'\left(\bar{k}_\rho^{e,h} r_b^{e,h}\right) \cdot H_n'^{(2)}\left(\bar{k}_\rho^{e,h} r_a^{e,h}\right) \right]_{\text{diag}} \\
{}_a &= T^e \Omega_n^e \chi_n^e \left(\bar{k}_\rho^e\right)^{-2} (T^e)^{-1} \bar{\varepsilon}_r^e - Q^h T^h \left(\gamma_n^h\right)^{-1} \\
&\quad \times s_n^h (T^h)^{-1} (\bar{Q}^e)^{-1} \\
{}_b &= -T^e \Omega_n^e s_n^e \left(\bar{k}_\rho^e\right)^{-2} (T^e)^{-1} \bar{\varepsilon}_r^e + T^h \left(\bar{k}_\rho^h\right)^{-2} \left(\gamma_n^h\right)^{-1} \\
&\quad \times T^h \chi_n^h (T^h)^{-1} (T^e)^{-1} (\bar{Q}^e)^{-1} \\
{}_t &= T^e \Omega_n^e \left(\bar{k}_\rho^e\right)^{-2} (T^e)^{-1} \bar{\varepsilon}_r^e + Q^h T^h \left(\gamma_n^h\right)^{-1} \\
&\quad \times (T^h)^{-1} (\bar{Q}^e)^{-1}.
\end{aligned}$$

REFERENCES

[1] J. Huang, "A Ka-band circularly polarized high gain microstrip array antenna," *IEEE Trans. Antennas Propagat.*, vol. 43, pp. 113–116, Jan. 1995.

[2] S. Kitao, M. Yamayo, H. Ohmine, H. Aoki, and T. Haruyama, "A radiation properties of triplate line fed microstrip array antenna with polarization grid in the 60-GHz," *IEICE Nat. Conv. Rec.*, vol. B-60, Sept. 1995.

[3] T. Yoneyama and S. Nishida, "Nonradiative dielectric waveguide for millimeter wave integrated circuits," *IEEE Trans. Microwave Theory Tech.*, vol. MTT-29, pp. 1188–1192, Nov. 1981.

[4] K. Wu, L. Ji, and R. G. Bosisio, "A low loss unidirectional dielectric radiator (UDR) for antenna and space power combing circuits," *IEEE Trans. Microwave Theory Tech.*, vol. 42, pp. 339–341, Feb. 1994.

[5] H. An, K. Wu, and R. G. Bosisio, "Analytic and experimental investigations of aperture coupled unidirectional dielectric radiator array (UDRA)," *IEEE Trans. Antennas Propagat.*, vol. 44, pp. 1201–1207, Sept. 1996.

[6] A. Sanchez and A. A. Oliner, "A new leaky waveguide for millimeter waves using nonradiative dielectric (NRD) waveguide—Part 2: Comparison with experiments," *IEEE Trans. Microwave Theory Tech.*, vol. 35, pp. 748–752, Sept. 1988.

[7] T. Yoneyama, T. Kowahara, and S. Nishida, "Experimental study of nonradiative dielectric waveguide leaky wave antenna," in *Proc. ISAP'85* Kyoto, Japan, 1985, pp. 85–88.

[8] K. Maamria, T. Wagatsuma, and T. Yoneyama, "Leaky NRD guide as a feeder for microwave planar antenna," *IEEE Trans. Antennas Propagat.*, vol. 41, pp. 1680–1686, Dec. 1993.

[9] M. Guglielmi and D. R. Jackson, "Broadside radiation from periodic leaky-wave antenna," *IEEE Trans. Antennas Propagat.*, vol. 41, pp. 31–37, Jan. 1993.

[10] H. An, K. Wu, and R. G. Bosisio, "Aperture coupled unidirectional dielectric radiator (UDR)," *Electron. Lett.*, vol. 31, pp. 145–146, Feb. 1995.

[11] Y. Kobayashi and S. Tanaka, "Resonant modes of a dielectric rod resonator short-circuited at both ends by parallel conducting plates," *IEEE Trans. Microwave Theory Tech.*, vol. MTT-28, pp. 1077–1085, Oct. 1980.

[12] J. E. Lee, G. M. Wilkons, and R. Mittra, "Finite-element analysis of axsiymetric cavity resonator using a hybrid edge element techniques," *IEEE Trans. Microwave Theory Tech.*, vol. 41, pp. 1981–1987, Nov. 1993.

[13] C. Di Nallo, F. Frezza, and A. Galli, "Full wave model analysis of arbitrarily shaped dielectric waveguides through an efficient boundary element method formulation," in *IEEE MTT-S Symp. Dig.*, Orlando, FL, 1995, pp. 479–482.

[14] K. Wu, R. Vahldieck, J. Fikart, and H. Minkus "The influence of finite conductor thickness and conductivity on fundamental and higher-order modes in miniature hybrid MIC's (MHMIC's) and MMIC's," *IEEE Trans. Microwave Theory Tech.*, vol. 41, pp. 421–430, Mar. 1993.

[15] K. Wu and R. Vahldieck, "Comprehensive MoL analysis of a class of semiconductor-based transmission lines suitable for microwave and optoelectric application," *Int. J. Numer. Modeling*, vol. 4, pp. 45–62, Jan. 1991.

Songxin Qi was born in Zhejiang, China, on November 25, 1965. He received the B.A.Sc. and M.A.Sc. degrees from Zhejiang University, Hanzhou, China, in 1986 and 1990, respectively, and the Ph.D. degree from Southeast University, Nanjing, China, in 1994, all in electrical engineering.

From June 1996 to Dec. 1997, he was with Polygrames Research Center, Department of Electrical and Computer Engineering, Ecole Polytechnique, Montréal, P.Q., Canada, as a Post-Doctoral Researcher. He is currently with the Broadband Wireless Networks Division, Northern Telecom (Nortel) Corporation, Winnipeg, Man., Canada. His current interest is in the design of power amplifiers, oscillators, and microwave and millimeter-wave subsystem.

Ke Wu (M'87–SM'92), for photograph and biography, see this issue, p. 1734.